

Laboratory and numerical studies were conducted to investigate the transport and release of *Escherichia coli* D21g in preferential flow systems with artificial macropores under different ionic strength (IS) conditions. Macropore length had a great impact on the preferential transport of *E. coli* D21g, especially under high-IS conditions, but discontinuous macropores had less preferential transport. At low IS, more extensive transport in the preferential path and earlier arrival time were observed for *E. coli* D21g than Br^- as a result of size exclusion.

Y. Wang and J. Šimůnek, Dep. of Environmental Sciences, Univ. of California, Riverside, CA 92521; and S. Bradford, USDA-ARS, U.S. Salinity Lab., Riverside, CA 92507. *Corresponding author (Ywang032@ucr.edu)

Vadose Zone J.
doi:10.2136/vzj2013.07.0120
Received 6 July 2013

© Soil Science Society of America
5585 Guilford Rd., Madison, WI 53711 USA.

All rights reserved. No part of this periodical may be reproduced or transmitted in any form or by any means, electronic or mechanical, including photocopying, recording, or any information storage and retrieval system, without permission in writing from the publisher.

Physicochemical Factors Influencing the Preferential Transport of *Escherichia coli* in Soils

Yusong Wang,* Scott A. Bradford, and Jiří Šimůnek

Laboratory and numerical studies were conducted to investigate the transport and release of *Escherichia coli* D21g in preferential flow systems with artificial macropores under different ionic strength (IS) conditions. Macropores were created by embedding coarse sand lenses in a fine sand matrix and altering the length, continuity, and vertical position of the lens. The length of an artificial macropore proved to have a great impact on the preferential transport of *E. coli* D21g, especially under high-IS conditions. A discontinuous macropore (interrupted by fine sand) was found to have less preferential transport of *E. coli* D21g than a continuous macropore of the same length that was open to either the top or bottom boundary. At low IS, more extensive transport in the preferential path and earlier arrival time were observed for *E. coli* D21g than Br^- as a result of size exclusion. Two release pulses (one from the preferential path and the other from the matrix) were observed following a reduction of the solution IS for flow systems with macropores that were open to either the top or bottom boundary, whereas three pulses (two from the preferential path and another from the matrix) were observed for systems with discontinuous macropores. Numerical simulations of *E. coli* D21g under both constant and transient solution chemistry conditions had very high agreement with the experiment data, except for their capability to predict some subtle differences in transport between the various lens configurations.

Abbreviations: BTC, breakthrough curve; DI, deionized; IS, ionic strength.

The vadose zone serves as an important barrier to protect groundwater from pathogenic microorganisms that can cause waterborne disease outbreaks (Runnells, 1976; National Research Council, 1994; Jamieson et al., 2002). The capability of the vadose zone to remove pathogens depends on properties of the porous media, the microbes, and the soil solution (Harvey and Garabedian, 1991; Tan et al., 1994; Tufenkji, 2007; Ding, 2010). An understanding and ability to simulate the influence of various factors that enhance the transport potential of pathogens in the vadose zone is especially needed to protect water resources from contamination. In this research, we considered three factors that are known to enhance the transport potential of microbes in soils: (i) preferential flow; (ii) transients in solution chemistry; and (iii) size exclusion.

Rapid water flow may occur in the vadose zone as a result of plant roots, burrowing earthworms, cracks, or natural structural heterogeneities (Wollum and Cassel, 1978; Beven and Germann, 1982; Madsen and Alexander, 1982; Unc and Goss, 2003; Cey et al., 2009). Accurate descriptions of contaminant transport in the vadose zone is hampered by these preferential flow pathways (Šimůnek et al., 2003) that bypass a large part of the soil matrix (Jury and Flühler, 1992). In particular, it is extremely difficult to characterize physical features (e.g., the length and configuration) of preferential flow pathways in natural systems and the exchange of water and contaminants at the interface between the preferential pathway and the soil matrix. Both of these factors are expected to have a critical influence on the transport and fate of contaminants in preferential flow systems but are still poorly

quantified (Harvey et al., 1993; Morley et al., 1998; Allaire-Leung et al., 2000a, 2000b; Allaire et al., 2002a, 2002b).

Many studies have investigated the transport of colloids and microorganisms in the field or in undisturbed soil columns with preferential flow (Bales et al., 1989; Dean and Foran, 1992; Jarvis, 2007; Pang et al., 2008; Cey et al., 2009; Cey and Rudolph, 2009; Guzman et al., 2009). Preferential pathways have been found to be a major contributor to the overall transport of microbes because they are typically strongly retained in the soil matrix (Bales et al., 1989; Abu-Ashour et al., 1994; Jiang et al., 2010). However, most of these researches are qualitative in nature because of the difficulty in quantifying the physical and chemical complexities of the soil matrix and macropore system. Studies using artificial macropores provide an opportunity to overcome many of these experimental and modeling limitations because the macropore geometry and hydraulic properties can be well defined and controlled (Fontes et al., 1991; Pivetz and Steenhuis, 1995; Castiglione et al., 2003; Guzman et al., 2009; Arora et al., 2011, 2012; Wang et al., 2013). However, systematic studies investigating the influence of the length and configuration of artificial macropores on the preferential transport of bacteria have not yet been reported.

Solution chemistry has proven to be an important factor that influences the transport and retention of microorganisms in porous media (Mills et al., 1994; Yee et al., 2000; Dong et al., 2002; Chen and Walker, 2007) and in systems with preferential flow (Fontes et al., 1991; Wang et al., 2013). The solution chemistry may change dramatically in the vadose zone during infiltration and drainage events as a result of differences in water quality at the soil surface (rain, irrigation, and runoff), evapotranspiration, and the mineral composition of the soil and groundwater. Such transients in solution chemistry are well known to induce the release of colloids and microbes in homogeneous porous media (Bales et al., 1989; McDowell-Boyer, 1992; Ryan and Gschwend, 1994; Nocito-Gobel and Tobiason, 1996; Roy and Dzombak, 1996; Grolimund et al., 2001; Lenhart and Saiers, 2003; Cheng and Saiers, 2009; Tosco et al., 2009; Bradford and Kim, 2010; Bradford et al., 2012). Consequently, transients in solution chemistry may jeopardize the purification capability of the vadose zone by inducing microbial release. There is presently a great need to understand processes that influence microbial remobilization, especially in soils with preferential flow. Wang et al. (2013) demonstrated that transients in solution chemistry can remobilize retained microbes and rapidly transport them in a preferential flow system. However, numerical modeling of this microbe release and transport has not yet been reported.

In addition to preferential flow and transients in solution chemistry, size exclusion may also enhance the transport potential of microbes in soils by physically restricting their transport to larger, more conductive pore spaces (Ryan and Elimelech, 1996; Ginn, 2002). It is possible that size exclusion will be more pronounced in

systems with preferential flow because of the wide difference in pore sizes between the soil matrix and the high-permeability domain. However, this issue has not yet been systematically investigated.

The objectives of this research were to: (i) investigate the influence of the length and configuration (as shown in Fig. 1) of artificial macropores on the preferential transport of microorganisms under different ionic strength (IS) conditions; (ii) simulate the release behavior of microbes with transients in solution chemistry in systems with preferential flow; and (iii) study the effect of size exclusion on microbial transport in systems with preferential flow. No attempt was made in this work to determine specific mechanisms of cell retention (e.g., attachment and straining) because of complications arising from preferential flow.

Experimental Information

Porous Media and Electrolyte Solutions

Two sizes of Ottawa (quartz) sand were used in the column experiments. The median grain sizes (d_{50}) of these sands were 120 and 710 μm . To eliminate any background interference from clay particles, the sand was treated by a salt cleaning procedure described by Bradford and Kim (2010).

Electrolyte solutions for the column experiments consisted of autoclaved, deionized (DI) ($\text{pH} = 5.8$) water with the IS adjusted to 0, 1, and 20 mmol L^{-1} using NaCl and NaBr to create a range of adhesive conditions between the bacteria and sand. The concentration of the conservative tracer Br was determined in the column effluent using a Br-selective electrode (Thermo Scientific Orion Br electrode Ionplus Sure-Flow).

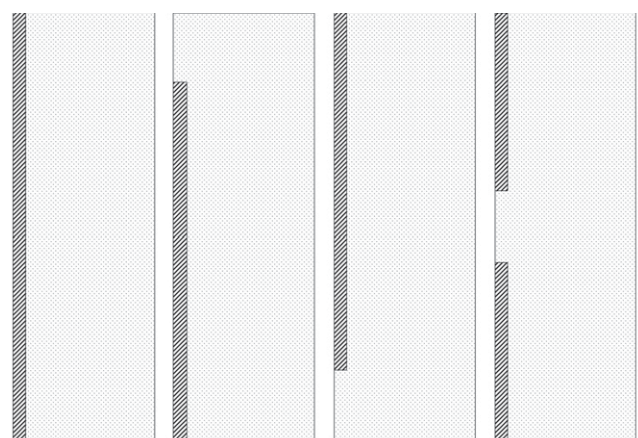


Fig. 1. Axisymmetric representation of the four types of sand lens structures (column center is on the left-hand side) studied in this research: Type I, one lens through the whole column; Type II, one lens open to the bottom boundary; Type III, one lens open to the top boundary; and Type IV, a discontinuous lens open to both boundaries (diagonal pattern represents coarse sand and point pattern represents fine sand).

***Escherichia coli* D21g**

We selected *E. coli* D21g, a Gram-negative, nonmotile bacterial strain (Walker et al., 2004), as a representative microorganism for the column transport experiments. The culture and harvest procedures used in this study have been described by Wang et al. (2013). In brief, *E. coli* D21g was cultured overnight (12–18 h) at 37°C in Luria-Bertani broth (LB broth, Fisher Scientific) containing 0.03 mg L⁻¹ gentamycin (Sigma), transferred onto an LB media plate containing 0.03 mg L⁻¹ gentamycin, and the plates were cultured overnight (12–18h) at 37°C. The colonies were harvested into sterile water, and then the bacterial suspension was centrifuged and resuspended two times to remove all traces of the growth medium. A fresh cell suspension at the desired electrolyte solution was prepared right before the start of each experiment. The concentrations of *E. coli* D21g in influent, effluent, and soil solution were determined using a spectrophotometer (Unico UV-200, United Products & Instruments) at 600 nm (Torkzaban et al., 2008) or with the spread plating method (American Public Health Association, 1989) when necessary (e.g., at low concentrations).

The NaBr solution containing *E. coli* D21g at a concentration of $\sim 1.0 \times 10^8$ cells mL⁻¹ was continuously mixed during the column experiment using a magnetic stirrer. The value of the influent concentration (C_0) was measured three times during the course of a transport experiment to assess the reproducibility of the measurements and microbial survival. The spectrophotometer readings for *E. coli* D21g were within 1% of C_0 , and the standard deviation of the spread plating method was 14.3% of C_0 . No systematic decrease in C_0 was observed during the column experiments, which indicates that little death occurred during this interval.

Column Experiments

Column experiments were conducted in a similar way to that described by Wang et al. (2013) with some modifications. Preferential transport experiments were conducted in an acrylic column that was 22 cm long and had an inside diameter of 13.2 cm. Preferential flow systems were created by packing fine (120- μ m) and coarse (710- μ m) sands into the column as follows: (i) the column was filled with autoclaved DI water to about one-third of the column height, and a 30-cm-long plastic tube with outside diameter of 1.14 cm was held in the center of the column; (ii) the fine sand was incrementally wet packed into the matrix portion of the column (outside the plastic tube) to a height of 20 cm; (iii) excess water in the plastic tube was drained from the bottom; (iv) the tube was carefully pulled out of the column without disturbing the surrounding fine matrix sand and leaving a 1.14-cm-diameter hole in the center of the column; (v) the hole was then filled to a height of 20 cm with various combinations of coarse and fine sands (Fig. 1), using a funnel, to create the desired preferential flow lens structure; and (vi) the column was then

saturated with water from the bottom. Four lens configurations were considered (Fig. 1) that are denoted as Types I (continuous coarse sand throughout the column), II (coarse sand lens of variable length that is open at the bottom boundary), III (coarse sand lens of variable length that is open at the top boundary), and IV (coarse sand lens of variable length that is open at both boundaries but discontinuous in the center).

A polyester membrane (Saatifil PES 18/13) with an 18- μ m nominal pore size was placed at the bottom of the column and connected to a hanging water column (tube) to control the bottom boundary pressure at 0 cm. Solutions were delivered onto the top boundary of the heterogeneous column at a steady flow rate using a rain simulator connected to a peristaltic pump. The water velocity was selected to just maintain saturated conditions (several millimeters of ponding at the surface) in the column through the experiments. The total Darcy velocity through the columns varied from 0.35 to 0.40 cm min⁻¹ for different lengths of lens. Two pore volumes (PVs) of a selected NaCl solution were flushed through the column, and the sand was allowed to equilibrate with this solution (Phase 0) before initiating a microbial transport experiment.

Microbial transport experiments were performed in two phases, with the same boundary conditions and flow velocity as in Phase 0. First, several PVs of microbe suspension and NaBr with the selected IS were introduced into the column at a constant rate (Phase I). Second, NaCl solution was flushed through the column at the same flow rate and IS as in Phase I until the effluent microbe concentration returned to a baseline level (Phase II). Effluent samples were continuously collected during the transport experiment at selected intervals using a fraction collector and then analyzed for Br and microbe concentrations as described above.

After completion of Phases I and II, some of the columns at IS = 20 mmol L⁻¹ underwent an additional experimental Phase III to examine the release of retained microbes with a reduction in solution IS. In this case, the columns were flushed with autoclaved DI water at the same velocity as during Phases I and II until the released microbe concentration in the effluent returned to a baseline level. The effluent samples were collected and analyzed using the same protocols as during Phases I and II.

The distribution of retained microbes in the heterogeneous columns was quantified after recovery of the breakthrough curves (BTCs) (Phases I and II) for the replicate transport experiments conducted with IS = 20 mmol L⁻¹ solutions but without Phase III. Sand samples were taken at seven depths (spaced according to the position of the lens) and three locations, namely: the lens, the matrix in the vicinity of the lens, and the bulk matrix. The length and position of preferential paths were determined during extraction. The sand samples were carefully excavated into tubes containing excess DI water. The tubes were shaken for 15 min to liberate any reversibly

Table 1. Model parameters from homogeneous column experiments presented in Wang et al. (2013).

Medium	Ionic strength	Dispersivity	Microbe release rate coefficient	Normalized solid-phase microbe conc.
	mmol L ⁻¹	cm	min ⁻¹	cm ³ g ⁻¹
Fine sand	1	0.10	0.0004	0.01
	20	0.10	0.2	3.5
Coarse sand	1	0.55	0	0
	20	0.55	0	0

retained microbes, and the concentrations of *E. coli* D21g in the excess solution were determined as described above.

Numerical Models

A two-dimensional finite element mathematic model was created using the COMSOL software package and used to simulate the transport, retention, and release of *E. coli* D21g in the heterogeneous column experiments based on the solution of the Richards equation and the advection–dispersion equation (ADE) with terms for kinetic retention and release. The microbial transport equations are

$$\frac{\partial(\theta C)}{\partial t} = \frac{\partial}{\partial x_i} \left(\theta D_{ij} \frac{\partial C}{\partial x_j} \right) - \frac{\partial q_i C}{\partial x_i} - \theta \psi k_{sw} C + \rho k_{rs} (S - f_c S_3) H_o (S - f_c S_3) \quad [1]$$

$$\frac{\partial(\rho S)}{\partial t} = \theta \psi k_{sw} C - \rho k_{rs} (S - f_c S_3) H_o (S - f_c S_3) \quad [2]$$

where subscripts i and j denote coordinate directions, C [N L⁻³, where N denotes number] is the microbe concentration in the aqueous phase, S [N M⁻¹] is the microbe concentration on the solid phase, S_3 [N M⁻¹] is the value of S before a reduction of the IS during Phase III, f_c (dimensionless) is the fraction of microbes on the solid phase that still remains immobilized after a reduction in IS, D_{ij} [L² T⁻¹] is the hydrodynamic dispersion coefficient, q_i [L T⁻¹] is the Darcy water velocity in the i th direction, k_{rs} [T⁻¹] is the microbe release rate coefficient, k_{sw} [T⁻¹] is the microbe retention rate coefficient, θ (dimensionless) is the soil water content, ρ [M L⁻³] is the soil bulk density, t [T] is time, x [L] is the spatial coordinate, and H_o is the Heaviside function that is equal to 0 when $S < f_c S_3$ and 1 when $S \geq f_c S_3$. The parameter ψ (dimensionless) accounts for time- and concentration-dependent blocking using a Langmuirian approach as (Adamczyk et al., 1994)

$$\psi = 1 - \frac{S}{S_{\max}} \quad [3]$$

where S_{\max} [N M⁻¹] is the maximum solid-phase concentration of microbes.

In addition to Eq. [1–3], the solution IS (1:1 electrolyte) was also simulated during Phase III using an ADE for a conservative tracer. The last term on the right-hand side of Eq. [1] and [2] accounts for the release of *E. coli* D21g with a reduction in IS during Phase III in a manner similar to Bradford et al. (2012). In the presence of DI water, k_{sw} was set equal to 0 based on data presented by Wang et al. (2013) for low-IS conditions, f_c was determined from mass balance information following the completion of Phase III, and k_{rs} was estimated by optimization (trial and error) to the experimental data. The value of S_3 was set according to the distribution of the solid-phase concentration of microbes at the end of Phase II. This approach allowed a known amount of retained *E. coli* D21g to be released on arrival of the DI water front at a particular location.

We followed a step-by-step procedure presented by Wang et al. (2013) to determine hydraulic properties and microbe retention parameters for simulations in preferential flow systems during Phases I and II. The saturated water content (θ) and bulk density (ρ) were calculated from experimental measurements to be 0.36 cm³ cm⁻³ and 1.7 g cm⁻³, respectively. The saturated hydraulic conductivities (K_s) of the matrix were determined from the breakthrough time of Br, which varied from 0.31 to 0.33 cm min⁻¹ due to slight differences in column packing. The saturated hydraulic conductivities of the coarse lenses were inversely estimated in HYDRUS 2D (Šimůnek et al., 2008) using the geometry information along with the total flow rate and the hydraulic conductivity of the matrix, which varied from 10.5 to 11.1 cm min⁻¹. The dispersivity (λ) and the retention parameters (S_{\max} , k_{sw} , and k_{rs}) for D21g in the coarse (lens) and fine (matrix) sands under the various solution chemistries are presented in Table 1. These parameters were determined from transport experiments conducted in homogeneous columns for similar sands, solution chemistries, and water velocities (Wang et al., 2013). In this case, $k_{rs} = 0$ and k_{sw} was a constant for the given solution chemistry conditions during Phases I and II.

Results and Discussion

Bromide

Figure 2 shows the normalized effluent concentrations (C/C_0) of Br as a function of time from columns with Type I and II lenses when the length of the coarse sand lens ranged from 10 to 20 cm. Two pulses of Br were observed at the outlet of all columns. The first pulse traveled through the lens and arrived much earlier than the second pulse from the matrix. The length of the lens had a great impact on the arrival times of the first pulse. Specifically, the arrival time of the first pulse increased from 2 to 12 min with

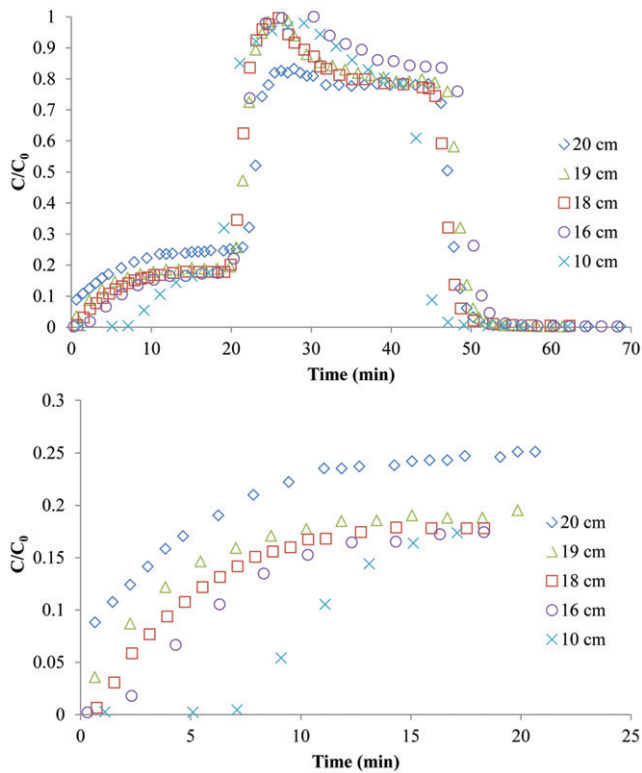


Fig. 2. Observed effluent concentrations of Br^- as a function of time for columns with Type I (20 cm) and Type II (19, 18, 16, and 10 cm) lens configurations. The bottom figure zooms on the early arrival of Br^- through the lens.

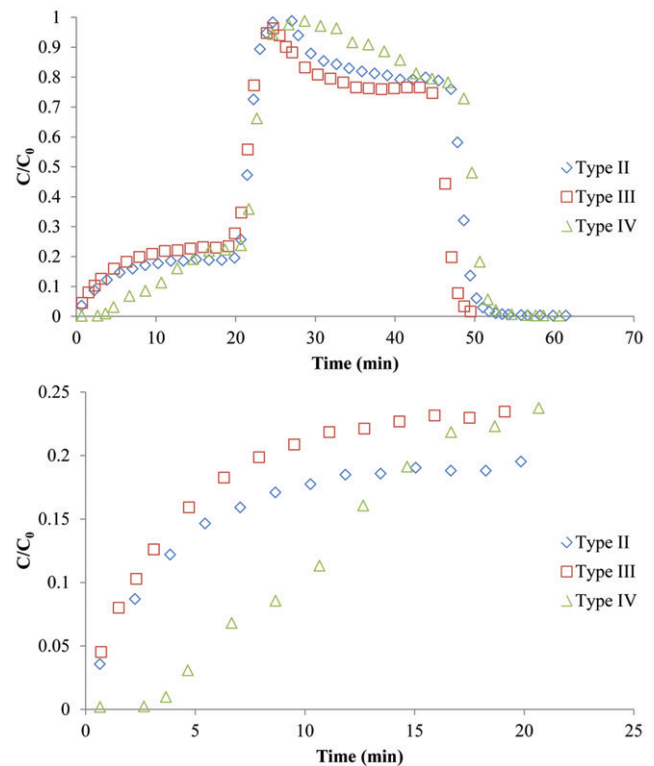


Fig. 3. Observed effluent concentrations of Br^- as a function of time for columns with the same lens length (19 cm) but with different lens configurations. The bottom figure zooms on the early arrival of Br^- through the lens.

a decrease in the length of the Type II lens from 20 to 10 cm, as shown in Table 2. Type III and IV lenses also exhibited this same trend (Table 2). As the length of the lens decreased, water and Br had to travel a longer distance through the fine sand, which decreased the average velocity of both water and Br and delayed the arrival of Br at the outlet. This decrease in velocity produced a corresponding decrease in the relative amount of Br that was transported through the preferential pathway (the first pulse) with a decrease in the lens length. Conversely, the velocity of the matrix was almost the same for all columns, and the arrival time of the second pulse was therefore similar (21.1–23.8 min).

The influence of the lens configuration (Types II, III, and IV) on Br transport when the lens length equaled 19 cm is shown in Fig. 3. Differences in the Br BTCs for Type II (lens continuous at the column bottom) and III (lens continuous at the column top) lens configurations were rather minor. Conversely, the Type IV (lens discontinuous in the center) lens configuration produced significantly different BTCs from Types II and III, especially with respect to the pulse from the preferential pathway (Fig. 3). The pulse of Br from the preferential path had more dispersion and arrived slightly later for Type IV heterogeneity than for the other two lens configurations. This observation indicates that the discontinuous lens created more disruptions to flow and transport pathways.

Table 2. Breakthrough information for Br.

Type of lens configuration	Length of lens cm	Arrival time of pulse		Peak conc. in first pulse ($100 \times C/C_0$)	Total recovery %
		of first pulse min	of second pulse min		
Type I	20	1.4	23.8	24.7	99.4
	19	3.2	21.9	19.5	99.6
Type II	18	3.7	21.5	17.8	100.1
	16	5.3	21.8	16.8	100.2
	10	11.1	21.1	16.3	98.9
Type III	19	3.1	22.2	20.6	99.5
Type IV	19	6.6	22.5	16.6	99.6

Escherichia coli D21g

Constant Solution Chemistry Conditions

A high energy barrier limited the retention of *E. coli* D21g in both fine and coarse sand when the IS equaled 1 mmol L^{-1} (Wang et al., 2013). Thus, the influence of lens length and configuration was very similar for *E. coli* D21g and Br with $\text{IS} = 1 \text{ mmol L}^{-1}$ (Fig. 4). Similar to Br, the first pulse of *E. coli* D21g arrived later and had less mass when the length of the

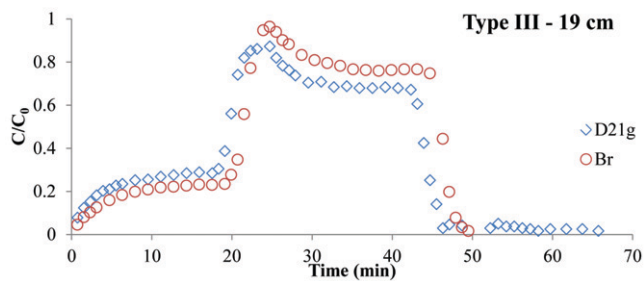


Fig. 4. Observed effluent concentrations of *E. coli* D21g at an ionic strength of 1 mmol L^{-1} and Br as a function of time for Type III lens configuration with a length of 19 cm.

lens decreased, and was more dispersed for Type IV than II and III lens configurations. Conversely, the arrival time for *E. coli* D21g in the second pulse (from the matrix) was about 1.5 min (0.07 pore volumes) earlier than for Br in the same experiments (Tables 2 and 3; Fig. 4). This observation was ascribed to size exclusion (Fontes et al., 1991; Ryan and Elimelech, 1996; Morley et al., 1998; Ginn, 2002), which can increase the transport velocity of particles by constraining them to larger pore networks. It was not possible to tell whether *E. coli* D21g also had an earlier arrival time than Br in the first pulse (lens) because of the very rapid arrival for both Br and *E. coli* D21g; however, the relative concentration of *E. coli* D21g was higher than that of Br in the first pulse (Tables 2 and 3). Because Br is a conservative tracer and some *E. coli* D21g was retained in the sand, this observation suggests that size exclusion may have also enhanced the transport of *E. coli* D21g in the lens in comparison to Br.

Figure 5 shows representative BTCs for *E. coli* D21g when the $\text{IS} = 20 \text{ mmol L}^{-1}$ and the lens configuration was Type I or II. In comparison to $\text{IS} = 1 \text{ mmol L}^{-1}$, the height of the energy barrier decreased and the depth of the secondary minimum increased when the $\text{IS} = 20 \text{ mmol L}^{-1}$ (Wang et al., 2013). Consequently, the retention of *E. coli* D21g in the fine matrix sand became much greater, and no detectable amount of *E. coli* D21g was transported through the 20-cm-long matrix (data not shown). However, *E. coli*

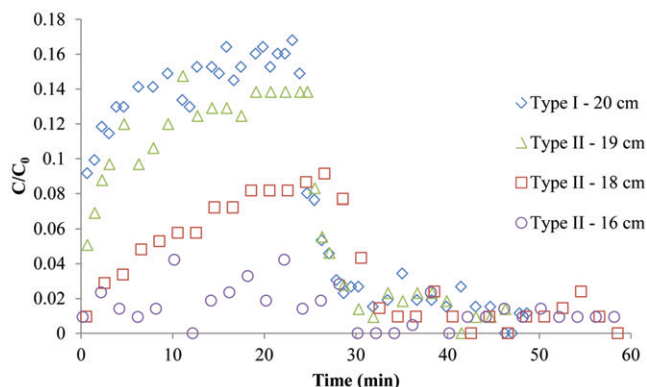


Fig. 5. Observed effluent concentrations of *E. coli* D21g at an ionic strength of 20 mmol L^{-1} as a function of time for Type I lens configuration (20 cm) and Type II lens configuration (19, 18, and 16 cm).

D21g was able to travel through the preferential path for most of the studied conditions, and the preferential flow pathway was the major or even the only route for *E. coli* D21g transport under high-IS conditions. The concentration of *E. coli* D21g in the effluent decreased dramatically when the lens length decreased, and only a trace amount of *E. coli* D21g was detected in the effluent when the lens length was 16 cm (Table 3). At $\text{IS} = 1 \text{ mmol L}^{-1}$, the lens length had no significant effect on the overall transport of *E. coli* D21g (Table 3). Consequently, the lens length had a much greater impact on the transport of *E. coli* D21g when the $\text{IS} = 20 \text{ mmol L}^{-1}$ than when the $\text{IS} = 1 \text{ mmol L}^{-1}$ (Table 3).

Figure 6 demonstrates that the transport of *E. coli* D21g was also influenced by the lens configuration (Types II and IV). In comparison with the Type II configuration, the Type IV heterogeneity enhanced the mixing and delayed the arrival of *E. coli* D21g in the first pulse when the $\text{IS} = 1 \text{ mmol L}^{-1}$. Similar behavior was observed for Br (Fig. 3). At a higher $\text{IS} = 20 \text{ mmol L}^{-1}$, the enhanced mixing of the two flow domains in the Type IV configuration produced greater retention of *E. coli* D21g in the preferential flow path and correspondingly less recovery of *E. coli* D21g in the first pulse (Table 3).

Table 3. Breakthrough information for *E. coli* D21g at 1 and 20 mmol L^{-1} .

Type of lens configuration	Length of lens cm	Ionic strength mmol L^{-1}	Arrival time	Arrival time of	Peak conc. in first pulse ($100 \times C/C_0$)	Total recovery %
			of first pulse	second pulse		
			min			
Type II	18	1	3.6	19.9	18.7	97.4
Type III	19	1	2.2	20.7	28.4	96.4
Type IV	19	1	3.0	21.4	24.5	96.5
Type III	19	20	2.3	NA	13.8	13.9
Type IV	19	20	3.0	NA	11.2	10.0
Type II	18	20	6.5	NA	9.1	8.2
Type II	16	20	NA	NA	4.2	2.9
Type IV	16	20	NA	NA	NA	0

The spatial distribution of the retained mass is also very important for understanding the transport and retention behavior of *E. coli* D21g in systems with preferential flow. Figure 7 shows representative retention profiles for *E. coli* D21g for Types II, III, and IV lens configurations when the lens length was 19 cm and the solution $\text{IS} = 20 \text{ mmol L}^{-1}$. Three locations were considered for each case: (i) in the lens

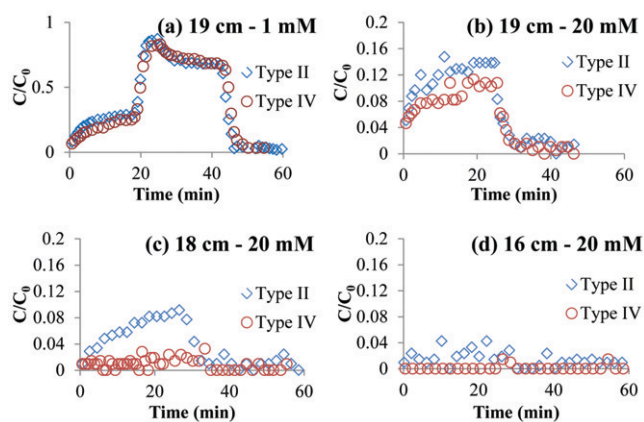


Fig. 6. Observed effluent concentrations of *E. coli* D21g for Type II and Type IV lens configurations as a function of time for (a) a lens length of 19 cm and an ionic strength (IS) of 1 mmol L⁻¹; (b) a lens length of 19 cm and an IS of 20 mmol L⁻¹; (c) a lens length of 18 cm and an IS of 20 mmol L⁻¹; and (d) a lens length of 16 cm and an IS of 20 mmol L⁻¹.

(including the fine sand); (ii) in the matrix adjacent to the lens; and (iii) in the bulk matrix sand.

In the matrix, most retained cells were in the top few centimeters of the column, and S/C_0 rapidly decreased with an increase in distance from the column inlet. Conversely, values of S/C_0 in the coarse-sand portions of the lenses were very low. For the Type II lens configuration, the fine sand disruption in the preferential path was located at the top. Thus, the value of S/C_0 was about the same as in the matrix at this location (Fig. 7a). For the Type III lens configuration, the fine sand disruption in the preferential path was located at the bottom, and the value of S/C_0 in this region was as high as that in the top matrix (Fig. 7b). For the Type IV lens configuration, a high value of S/C_0 was located in the middle of the preferential flow path where the fine-sand disruption occurred (Fig. 7c).

The greatest amount of cell retention tended to occur in the matrix adjacent to the lens. This location reflects the influence of mass exchange between the lens and matrix, as well as retention in the matrix. Similar high values of S/C_0 occurred near the column inlet for the three lens configurations because retention was mainly controlled by the matrix in this location. Conversely, distinct differences in the amount of cell retention occurred with increasing depth for the various lens configurations because of differences in the amount of mass transfer between the lens and matrix. The higher values of S/C_0 with increasing depth in the Type III and IV configurations indicates that discontinuities to lenses that are open at the column top will increase the subsequent mass transfer from the lens to the matrix and thereby enhance *E. coli* D21g retention. On the other hand, cell retention adjacent to the lens in the Type II configuration was lower because the

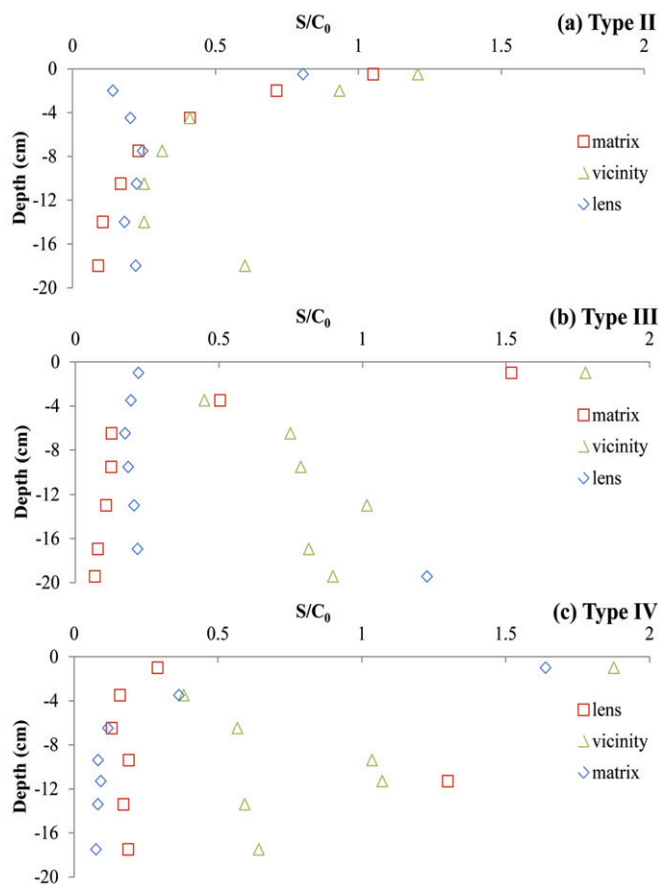


Fig. 7. Normalized solid-phase concentrations (S/C_0) of *E. coli* D21g as a function of depth for an ionic strength of 20 mmol L⁻¹ (Phases I and II), lens length of 19 cm, and lens configurations of (a) Type II, (b) Type III, and (c) Type IV for three locations: in the lens, in the matrix in the immediate vicinity of the lens, and in the matrix away from the lens.

cells had to initially travel through the matrix, and many were therefore retained in the matrix before reaching the lens.

Transients in Solution Chemistry

Figure 8 presents the release behavior of *E. coli* D21g during Phase III when the influent solution IS was switched from 20 mmol L⁻¹ to DI water. Type II, III, and IV lens configurations were considered, and the lens length was 16 cm. Table 4 gives the arrival times and mass balance information for the release process. Release was initiated during Phase III when the IS = 20 mmol L⁻¹ solution was replaced by DI water, and the secondary minimum was eliminated. Similar to transport during Phases I and II, multiple pulses of released cells were observed during Phase III because of preferential flow. The largest pulse of released *E. coli* D21g was about five times C_0 and arrived at the outlet about 21 min after the start of DI water flushing. This arrival corresponds with the travel time of Br through the matrix (Fig. 2 and 3). Consequently, this high peak reflects cell release from the matrix, where most of the cells were retained (Fig. 7). Conversely, the smaller earlier pulses mainly reflect mass transfer from the matrix to the lens because

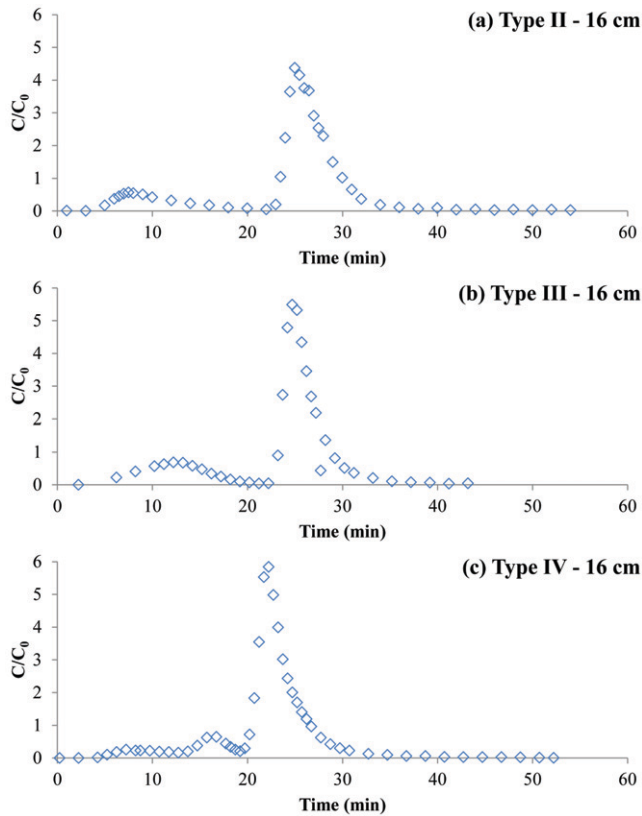


Fig. 8. Observed effluent concentrations of *E. coli* D21g as a function of time during the release process for (a) Type II lens of 16-cm length; (b) Type III lens of 16-cm length; and (c) Type IV lens of 16-cm length. The time when the influent solution was switched from 20 mmol L⁻¹ solution to deionized water was labeled as 0 at the start of Phase III.

little cell retention occurred in the coarse sand lens at IS = 20 mmol L⁻¹ (Wang et al., 2013). The lens configuration (Types II, III, and IV) had a significant influence on the number and magnitude of these earlier pulses. There was only one small pulse of released *E. coli* D21g for Type II and III lens configurations at earlier times (6.9–7.2 min), whereas the Type IV configuration produced two small pulses that arrived after 6.2 and 14.7 min. This observation suggests that mass transfer from the matrix to the lens was more efficient (easier) in the Type II and III configurations and less efficient in the discontinuous Type IV configuration.

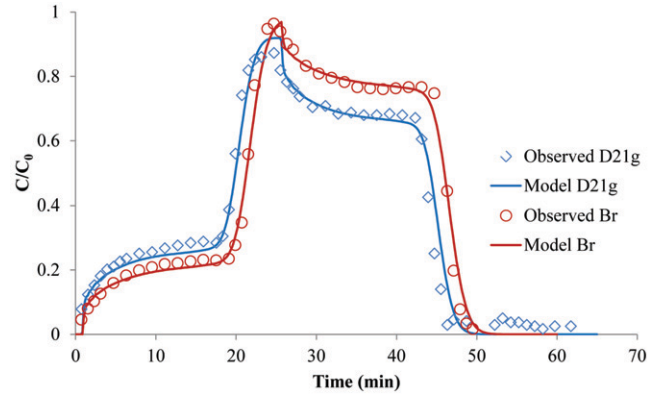


Fig. 9. Examples of observed and simulated effluent concentrations as a function of time for Br and *E. coli* D21g for a Type III lens with a 19-cm length and an ionic strength of 1 mmol L⁻¹.

Simulations with Numerical Models

Figure 9 shows examples of observed and simulated BTCs of Br and *E. coli* D21g at IS = 1 mmol L⁻¹ during Phases I and II. Figure 10 shows examples of observed and simulated BTCs of *E. coli* D21g at IS = 20 mmol L⁻¹ during Phases I and II along with cell release during Phase III when the IS was reduced to DI water. The model was able to simulate the transport of Br and *E. coli* D21g with very high accuracy during Phases I and II when the IS was 1 or 20 mmol L⁻¹. The release behavior of *E. coli* D21g from the matrix (the high-concentration pulse that arrived at later times) and the earlier pulse for Type II and III configurations were also well simulated by the model. Conversely, the model was not able to capture the subtle differences in the early release behavior for Type II, III, and IV configurations. In particular, the model failed to predict the enhanced dispersion during Phases I and II and the arrival times of the two earlier pulses associated with mass transfer from the matrix to the lens in the Type IV configuration. These differences may arise because cell retention processes that occurred at textural interfaces were incompletely quantified in the model (Bradford and Bettahar, 2005).

Summary and Conclusions

The length of the lens affected the water flow and transport of Br and *E. coli* D21g. In particular, a decrease in the lens length produced later arrival times and lower effluent concentrations through

Table 4. Release information for *E. coli* D21g.

Type of lens configuration	Length of lens	Arrival time of first small pulse	Arrival time of second small pulse	Peak conc. of first small pulse (100 × C/C ₀)	Peak conc. of second small pulse (100 × C/C ₀)	Recovery of first or first and second pulse	Arrival time of major pulse	Peak conc. of major pulse (100 × C/C ₀)	Recovery of major pulse
	cm	min				%	min		%
Type II	16	6.9	NA†	56.4	NA	17.8	23.0	437.5	78.0
Type III	16	7.2	NA	68.3	NA	22.4	23.2	548.7	69.5
Type IV	16	6.2	14.7	25.3	64.2	14.6	20.7	583.9	76.8

† NA, not applicable.

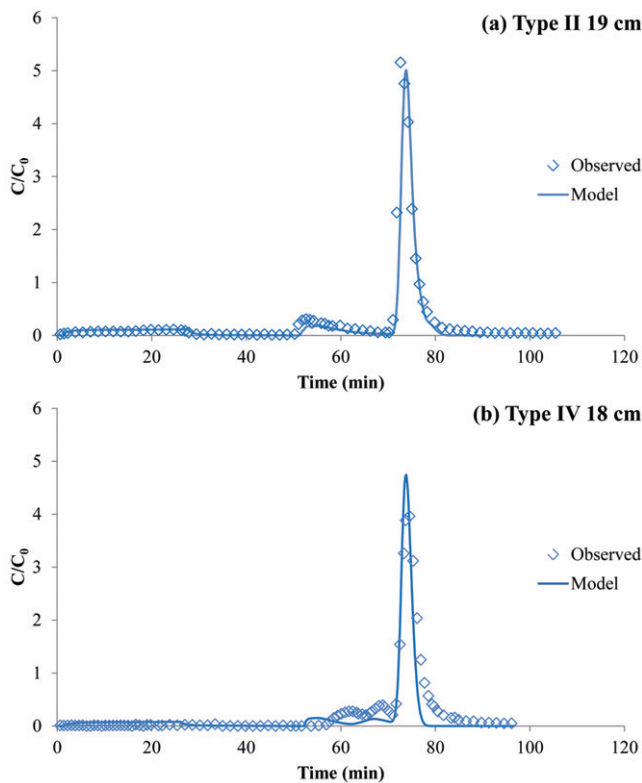


Fig. 10. Examples of observed and simulated effluent concentrations of *E. coli* D21g as a function of time for (a) a Type II lens of 19-cm length and (b) a Type IV lens of 18-cm length. The ionic strength was 20 mmol L⁻¹ during Phases I and II.

the preferential pathway. This effect became more pronounced for *E. coli* D21g at a high IS because of increased cell retention in the matrix. The Type IV (lens is discontinuous in the center) lens configuration produced a larger dispersivity and later arrival time in the preferential path than Type II (lens is open at the bottom) and III (lens is open at the top) configurations, and it also yielded less transport of *E. coli* D21g at high IS due to enhanced mixing of the flow through the preferential path and matrix compared with the other two configurations. Size exclusion not only increased the travel speed of *E. coli* D21g in both the matrix and preferential path but also increased the relative amount of *E. coli* D21g that was transported in the preferential path in comparison to Br.

Numerical simulations of *E. coli* D21g under both constant and transient solution chemistry conditions had very high agreement with the experiment data. However, the model wasn't capable of simulating some of the subtle differences in transport between the various lens configurations. In particular, the model could not simulate the enhanced dispersion behavior in the early preferential flow pulse for the Type IV configuration during Phases I and II. It also failed to predict the arrival times and transport amounts in the two earlier release peaks during Phase III for the Type IV configuration. Hence, model improvements are needed to better characterize cell transport and retention processes at the interface between the preferential path and matrix.

Acknowledgments

We would like to acknowledge Teresa Clapp for her help in conducting some of the transport experiments. This research was supported by the USDA-ARS, NP 214. The USDA is an equal opportunity provider and employer.

References

- Abu-Ashour, J., D.M. Joy, H. Lee, H.R. Whiteley, and S. Zelin. 1994. Transport of microorganisms through soil. *Water Air Soil Pollut.* 75:141–158. doi:10.1007/BF01100406
- Adamczyk, Z., B. Siwek, M. Zembala, and P. Belouschek. 1994. Kinetics of localized adsorption of colloid particles. *Adv. Colloid Interface Sci.* 48:151:280. doi:10.1016/0001-8686(94)80008-1
- Allaire, S.E., S.C. Gupta, J. Nieber, and J.F. Moncrief. 2002a. Role of macropore continuity and tortuosity on solute transport in soils: 1. Effects of initial and boundary conditions. *J. Contam. Hydrol.* 58:299–321. doi:10.1016/S0169-7722(02)00035-9
- Allaire, S.E., S.C. Gupta, J. Nieber, and J.F. Moncrief. 2002b. Role of macropore continuity and tortuosity on solute transport in soils: 2. Interactions with model assumptions for macropore description. *J. Contam. Hydrol.* 58:283–298. doi:10.1016/S0169-7722(02)00034-7
- Allaire-Leung, S.E., S.C. Gupta, and J.F. Moncrief. 2000a. Water and solute movement in soil as influenced by macropore characteristics: 1. Macropore continuity. *J. Contam. Hydrol.* 41:283–301. doi:10.1016/S0169-7722(99)00079-0
- Allaire-Leung, S.E., S.C. Gupta, and J.F. Moncrief. 2000b. Water and solute movement in soil as influenced by macropore characteristics: 2. Macropore tortuosity. *J. Contam. Hydrol.* 41:303–315. doi:10.1016/S0169-7722(99)00074-1
- American Public Health Association. 1989. Method 9222C: Delayed-incubation standard coliform procedure. In: *Standard methods for the examination of water and wastewater*. 17th ed. APHA, Washington, DC. p. 9-91–9-93.
- Arora, B., B.P. Mohanty, and J.T. McGuire. 2011. Inverse estimation of parameters for multidomain flow models in soil columns with different macropore densities. *Water Resour. Res.* 47:W04512. doi:10.1029/2010wr009451
- Arora, B., B.P. Mohanty, and J.T. McGuire. 2012. Uncertainty in dual permeability model parameters for structured soils. *Water Resour. Res.* 48:W01524. doi:10.1029/2011wr010500
- Bales, R.C., C.P. Gerba, G.H. Grondin, and S.L. Jensen. 1989. Bacteriophage transport in sandy soil and fractured tuff. *Appl. Environ. Microbiol.* 55:2061–2067.
- Beven, K., and P. Germann. 1982. Macropores and water flow in soils. *Water Resour. Res.* 18:1311–1325. doi:10.1029/WR018i005p01311
- Bradford, S.A., and M. Bettahar. 2005. Straining, attachment, and detachment of *Cryptosporidium* oocysts in saturated porous media. *J. Environ. Qual.* 34:469–478. doi:10.2134/jeq2005.0469
- Bradford, S.A., and H. Kim. 2010. Implications of cation exchange on clay release and colloid-facilitated transport in porous media. *J. Environ. Qual.* 39:2040–2046. doi:10.2134/jeq2010.0156
- Bradford, S.A., S. Torzaban, H. Kim, and J. Šimůnek. 2012. Modeling colloid and microorganism transport and release with transients in solution ionic strength. *Water Resour. Res.* 48:W09509.
- Castiglione, P., B. Mohanty, P. Shouse, J. Šimůnek, M.Th. van Genuchten, and A. Santini. 2003. Lateral water diffusion in an artificial macroporous system. *Vadose Zone J.* 2:212–221.
- Cey, E.E., and D.L. Rudolph. 2009. Field study of macropore flow processes using tension infiltration of a dye tracer in partially saturated soils. *Hydrol. Processes* 23:1768–1779. doi:10.1002/hyp.7302
- Cey, E.E., D.L. Rudolph, and J. Passmore. 2009. Influence of macroporosity on preferential solute and colloid transport in unsaturated field soils. *J. Contam. Hydrol.* 107:45–57. doi:10.1016/j.jconhyd.2009.03.004
- Chen, G.X., and S.L. Walker. 2007. Role of solution chemistry and ion valence on the adhesion kinetics of groundwater and marine bacteria. *Langmuir* 23:7162–7169. doi:10.1021/la0632833
- Cheng, T., and J.E. Saiers. 2009. Mobilization and transport of in situ colloids during drainage and imbibition of partially saturated sediments. *Water Resour. Res.* 45:W08414.
- Dean, D.M., and M.E. Foran. 1992. The effect of farm liquid waste application on tile drainage. *J. Soil Water Conserv.* 47:368–369.
- Ding, D. 2010. Transport of bacteria in aquifer sediment: Experiments and modeling. *Hydrogeol. J.* 18:669–679. doi:10.1007/s10040-009-0559-3

- Dong, H., T.C. Onstott, M.F. DeFlaun, M.E. Fuller, T.D. Scheibe, S.H. Streger, et al. 2002. Relative dominance of physical versus chemical effects on the transport of adhesion-deficient bacteria in intact cores from South Oyster, Virginia. *Environ. Sci. Technol.* 36:891–900. doi:10.1021/es010144t
- Fontes, D.E., A.L. Mills, G.M. Hornberger, and J.S. Herman. 1991. Physical and chemical factors influencing transport of microorganisms through porous media. *Appl. Environ. Microbiol.* 57:2473–2481.
- Ginn, T.R. 2002. A travel time approach to exclusion on transport in porous media. *Water Resour. Res.* 38(4). doi:10.1029/2001WR000865
- Grolmund, D., K. Barmettler, and M. Borkovec. 2001. Release and transport of colloidal particles in natural porous media: 2. Experimental results and effects of ligands. *Water Resour. Res.* 37:571–582. doi:10.1029/2000WR900286
- Guzman, J.A., G.A. Fox, R.W. Malone, and R.S. Kanwar. 2009. Transport from surface-applied manure to subsurface drains through artificial biopores. *J. Environ. Qual.* 38:2412–2421. doi:10.2134/jeq2009.0077
- Harvey, R.W., and S.P. Garabedian. 1991. Use of colloid filtration theory in modeling movement of bacteria through a contaminated sandy aquifer. *Environ. Sci. Technol.* 25:178–185. doi:10.1021/es00013a021
- Harvey, R.W., N.E. Kinner, D. MacDonald, D.W. Metzge, and A. Bunn. 1993. Role of physical heterogeneity in the interpretation of small-scale laboratory and field observations of bacteria, microbial-sized microsphere, and bromide transport through aquifer sediments. *Water Resour. Res.* 29:2713–2721. doi:10.1029/93WR00963
- Jamieson, R., R. Gordon, K. Sharples, G. Stratton, and A. Madani. 2002. Movement and persistence of fecal bacteria in agricultural soils and subsurface drainage water: A review. *Can. Biosyst. Eng. J.* 44:1–9.
- Jarvis, N.J. 2007. A review of non-equilibrium water flow and solute transport in soil macropores: Principles, controlling factors and consequences for water quality. *Eur. J. Soil Sci.* 58:523–546. doi:10.1111/j.1365-2389.2007.00915.x
- Jiang, S., L.P. Pang, G.D. Buchan, J. Šimůnek, M.J. Noonan, and M.E. Close. 2010. Modeling water flow and bacterial transport in undisturbed lysimeters under irrigations of dairy shed effluent and water using HYDRUS-1D. *Water Res.* 44:1050–1061. doi:10.1016/j.watres.2009.08.039
- Jury, W.A., and H. Flüher. 1992. Transport of chemicals through soil: Mechanisms, models, and field applications. *Adv. Agron.* 47:141–201. doi:10.1016/S0065-2113(08)60490-3
- Lenhart, J.J., and J.E. Saiers. 2003. Colloid mobilization in water-saturated porous media under transient chemical conditions. *Environ. Sci. Technol.* 37:2780–2787. doi:10.1021/es025788v
- Madsen, E.L., and M. Alexander. 1982. Transport of *Rhizobium* and *Pseudomonas* through soil. *Soil Sci. Soc. Am. J.* 46:557–560. doi:10.2136/sssaj1982.03615995004600030023x
- McDowell-Boyer, L.M. 1992. Chemical mobilization of micron-sized particles in saturated porous media under steady flow conditions. *Environ. Sci. Technol.* 26:586–593. doi:10.1021/es00027a023
- Mills, A.L., J.S. Herman, G.M. Hornberger, and T.H. Dejesus. 1994. Effect of solution ionic strength and iron coatings on mineral grains on the sorption of bacterial cells to quartz sand. *Appl. Environ. Microbiol.* 60:3300–3306.
- Morley, L.M., G.M. Hornberger, A.L. Mills, and J.S. Herman. 1998. Effects of transverse mixing on transport of bacteria through heterogeneous porous media. *Water Resour. Res.* 34:1901–1908. doi:10.1029/98WR01210
- National Research Council. 1994. Ground water recharge using waters of impaired quality. Natl. Acad. Press, Washington, DC.
- Nocito-Gobel, J., and J.E. Tobiasson. 1996. Effects of ionic strength on colloid deposition and release. *Colloids Surf. A* 107:223–231. doi:10.1016/0927-7757(95)03340-8
- Pang, L., M. McLeod, J. Aislabie, J. Šimůnek, M. Close, and R. Hector. 2008. Modeling transport of microbes in ten undisturbed soils under effluent irrigation. *Vadose Zone J.* 7:97–111. doi:10.2136/vzj2007.0108
- Pivetz, B., and T. Steenhuis. 1995. Soil matrix and macropore biodegradation of 2,4-D. *J. Environ. Qual.* 24:564–570. doi:10.2134/jeq1995.00472425002400040002x
- Roy, S.B., and D.A. Dzombak. 1996. Colloid release and transport processes in natural and model porous media. *Colloids Surf. A* 107:245–262. doi:10.1016/0927-7757(95)03367-X
- Runnells, D.D. 1976. Wastewaters in the vadose zone of arid regions: Geochemical interactions. *Ground Water* 14:374–385. doi:10.1111/j.1745-6584.1976.tb03131.x
- Ryan, J.N., and M. Elimelech. 1996. Colloid mobilization and transport in groundwater. *Colloids Surf. A* 107:1–56. doi:10.1016/0927-7757(95)03384-X
- Ryan, J.N., and P.M. Gschwend. 1994. Effects of ionic strength and flow rate on colloid release: Relating kinetics to intersurface potential energy. *J. Colloid Interface Sci.* 164:21–34. doi:10.1006/jcis.1994.1139
- Šimůnek, J., N.J. Jarvis, M.Th. van Genuchten, and A. Gärdenäs. 2003. Review and comparison of models for describing non-equilibrium and preferential flow and transport in the vadose zone. *J. Hydrol.* 272:14–35. doi:10.1016/S0022-1694(02)00252-4
- Šimůnek, J., M.Th. van Genuchten, and M. Šejna. 2008. Development and applications of the HYDRUS and STANMOD software packages and related codes. *Vadose Zone J.* 7:587–600. doi:10.2136/vzj2007.0077
- Tan, Y., J. Gannon, P. Baveye, and M. Alexander. 1994. Transport of bacteria in an aquifer sand: Experiments and model simulations. *Water Resour. Res.* 30:3243–3252. doi:10.1029/94WR02032
- Torkzaban, S., S.S. Tazehkand, S.L. Walker, and S.A. Bradford. 2008. Transport and fate of bacteria in porous media: Coupled effects of chemical conditions and pore space geometry. *Water Resour. Res.* 44:W04403. doi:10.1029/2007wr006541
- Tosco, T., A. Tiraferri, and R. Sethi. 2009. Ionic strength dependent transport of microparticles in saturated porous media: Modeling mobilization and immobilization phenomena under transient chemical conditions. *Environ. Sci. Technol.* 43:4425–4431. doi:10.1021/es900245d
- Tufenkji, N. 2007. Modeling microbial transport in porous media: Traditional approaches and recent developments. *Adv. Water Resour.* 30:1455–1469. doi:10.1016/j.advwatres.2006.05.014
- Unc, A., and M.J. Goss. 2003. Movement of faecal bacteria through the vadose zone. *Water Air Soil Pollut.* 149:327–337. doi:10.1023/A:1025693109248
- Walker, S.L., J.A. Redman, and M. Elimelech. 2004. Role of cell surface lipopolysaccharides in *Escherichia coli* K12 adhesion and transport. *Langmuir* 20:7736–7746. doi:10.1021/la049511f
- Wang, Y., S.A. Bradford, and J. Šimůnek. 2013. Transport and fate of microorganisms in soils with preferential flow under different solution chemistry conditions. *Water Resour. Res.* 49:2424–2436. doi:10.1002/wrcr.20174
- Wollum, A., and D. Cassel. 1978. Transport of microorganisms in sand columns. *Soil Sci. Soc. Am. J.* 42:72–76. doi:10.2136/sssaj1978.03615995004200010016x
- Yee, N., J.B. Fein, and C.J. Daughney. 2000. Experimental study of the pH, ionic strength, and reversibility behavior of bacteria–mineral adsorption. *Geochim. Cosmochim. Acta* 64:609–617. doi:10.1016/S0016-7037(99)00342-7